# Coherent interferometric imaging for synthetic aperture radar in the presence of noise

**Josselin Garnier[1] and Knut Sølna[2]**

[1] Laboratoire de Probabilités et Modèles Aléatoires and Laboratoire Jacques-Louis Lions,
Université Paris VII, 2 Place Jussieu, 75251 Paris Cedex 5, France
[2] Department of Mathematics, University of California, Irvine, CA 92697, USA

E-mail: garnier@math.jussieu.fr and ksolna@math.uci.edu

**Abstract**
This paper shows that the coherent interferometric imaging strategy originally
proposed in the context of passive or active arrays of antennas can be
implemented for synthetic aperture radar, in which a single antenna is used
as an emitter and as a receiver at successive positions along a trajectory.
The idea is to backpropagate the cross correlations of the recorded signals
over selected frequency-spatial windows rather than the signals themselves.
The theoretical analysis shows that the signal-to-noise ratio can be enhanced
dramatically compared to the standard matched filter processing, without any
loss of resolution. This holds true when the fluctuations of the recorded signals
have a spatial correlation (along the antenna trajectory) that is larger than the
distance between two successive positions of the antenna and smaller than the
length of the antenna trajectory. As a result, a good compromise between
resolution and deblurring can be achieved by an appropriate choice of the
spatial window size.

(Some figures in this article are in colour only in the electronic version)

## 1. Introduction

Synthetic aperture radar (SAR) is a technique currently used to do imaging from a satellite or
a plane emitting and recording electromagnetic waves [5, 9, 10]. In the SAR configuration an
antenna moves along a known trajectory and emits a train of pulses. The waves are scattered
by the probed region and the backscattered waves are detected by the same antenna. SAR can
be described mathematically by a simple antenna model and a single-scattering approximation
[8, 18]. The received signals are then used to produce an image. The imaging process consists
of a matched filter that backpropagates the signals to a test point in a virtual homogeneous
medium. Very high-resolution images can be obtained, for which the resolution corresponds

to that obtained by an array of antennas whose width would be equivalent to the length of the antenna trajectory. However SAR is very sensitive to noise, since it is critical to record the phases of the waves with high accuracy. In SAR acquisition there may be several noise sources. First, the positions of the antenna can be identified only with a relative precision. As it is typically a flight path or a satellite path, deviations from the nominal trajectory are more or less unavoidable. Second, the background medium may have propagation speed fluctuations. These two first phenomena can be modeled by assuming that the travel time for a round trip from the theoretical positions of the antenna to the target is random. Third, backscattering from a random collection of small scatterers (clutter) can give noise in the recorded signals that can be modeled by an additive white or colored Gaussian noise. Other sources of noise can be encountered [9].

SAR, being a high-resolution coherent imaging technique exploiting phase information, is particularly sensitive to phase errors. Many signal processing or analytic procedures which focus on explicit removal of such phase errors have been proposed and implemented to deblurr SAR images [6, 22]. In particular, the widely used phase gradient autofocus (PGA) technique aims at removing a large part of the phase errors [7, 12, 21] and can be implemented for various migration procedures [20]. The PGA technique exploits redundancy in order to compensate for phase errors, even in the presence of additive noise. With redundancy we here mean that many observations involve the same phase error. In the SAR context this situation may occur when (1) many high-contrast target points reflect signals above the noise level and (2) the phase errors are range independent, or equivalently target independent. In a situation with redundancy the PGA method is efficient because it averages the estimates of the phase errors over many targets to give high accuracy. It is in fact optimal in order to compensate for range-independent phase errors in the presence of small additive white noise [12]. However, if there are only one or a few target points in the medium, or there are many targets, but the additive noise is so strong that only one or a few targets are above the noise level, then redundancy is lost. Moreover, if the phase errors are range dependent, then it is necessary to break the search window into smaller sub-windows so that the errors present in each sub-window are approximately range invariant and hence, conventional autofocus procedures can be applied to each sub-window. If the dependence is strong and the sub-windows are small, then redundancy is lost [17]. It is then necessary to implement a more robust strategy. In this paper we introduce a method that does not require redundancy, which can address strong additive white noise and range-dependent phase errors, and that does not aim at explicitly estimating the phase error.

Recently coherent interferometric (CINT) imaging has been shown to achieve a good compromise between resolution and deblurring in noisy environments [1, 3]. It involves backpropagating the cross correlations of the recorded signals over appropriate space-time or space–frequency windows rather than the signals themselves. The choice of the sizes of the windows is the critical point since it allows one to select only the coherent contributions of the imaging process. It has been used to process data sets obtained from active or passive arrays of antennas using wave signals propagating through a heterogeneous medium [2, 4].

In this paper, we propose a CINT implementation for SAR imaging. In section 2, the conventional matched filter processing used in SAR is recalled and expressed in a suitable way in order to introduce in section 3 the CINT strategy. The resolution and noise properties of the CINT strategy in the context of SAR are studied and numerical simulations illustrating its performance are presented in section 4.

## 2. Matched filter processing

In the classical SAR setup, an antenna located in a plane or a satellite moves along a straight trajectory. At regularly spaced positions $\mathbf{x}_n$, $n = 1, \ldots, N$ along this trajectory and at regularly spaced times $nT$, the antenna emits an electromagnetic pulse $s(t - nT)$ that is reflected by the scatterers present in the medium, and the scattered wave $R_n(t)$ is detected by the same antenna. The collection of received signals $(R_n(t))_{t,n}$ is then used to produce an image. In this section, we give a simple but accurate model that describes the measured signals, and also present the usual imaging process.

The source signal used by the antenna is the chirped pulse

$$s(t) = \frac{1}{2} a \left( \frac{t}{T_p} \right) e^{-i\omega_c t - i\pi \gamma t^2}, \tag{1}$$

where $\omega_c$ is the carrier (angular) frequency, $\gamma$ is the chirp parameter, $a(t)$ is the normalized pulse shape function, and $T_p$ is the pulse width. For instance, we may have $a(t) = \exp(-t^2)$ or $a(t) = \mathbf{1}_{[-1,1]}(t)$. The choice of a chirped pulse results from a compromise between two requirements [8]. First, the range resolution of the system improves with increased bandwidth, as we shall see in the next sections. Thus, we would like to use short pulses. Second, the emitted field is limited in practice by the maximal power radiated by the antenna. Thus, short pulses have low energy and backscattered signals are buried in the noise. Therefore, SAR systems use pulse modulation of the form (1), so that the emitted pulse is a long waveform. The received signals are then compressed in order to synthesize the response of a short pulse. In this paper it is assumed that the following assumption is satisfied.

**Assumption 2.1.** $\omega_c \gg \pi \gamma T_p \gg T_p^{-1}$

This is a typical scaling for SAR configurations (see appendix). It means that the carrier frequency is large compared to the chirp bandwidth, which in turn is large compared to the pulse shape bandwidth, that is, we are in a situation with a high carrier frequency and a strong chirp. Indeed, in the case $a(t) = \exp(-t^2)$, the chirped pulse (1) has a Gaussian form, so that its Fourier transform can be computed explicitly:

$$\hat{s}(\omega) = \frac{T_p \sqrt{\pi}}{2\sqrt{1 + i\pi \gamma T_p^2}} \exp \left( -\frac{(\omega - \omega_c)^2 T_p^2}{4(1 + \pi^2 \gamma^2 T_p^4)} + i\frac{(\omega - \omega_c)^2 \pi \gamma T_p^4}{4(1 + \pi^2 \gamma^2 T_p^4)} \right),$$

which shows that the bandwidth is $2T_p^{-1}\sqrt{1 + \pi^2 \gamma^2 T_p^4} \simeq 2\pi \gamma T_p$ in the regime $\pi \gamma T_p \gg T_p^{-1}$. Here and throughout the paper the Fourier transform of a function $f(t)$ is denoted by $\hat{f}(\omega)$ and is defined by

$$\hat{f}(\omega) = \int f(t) e^{i\omega t} \, dt. \tag{2}$$

For an arbitrary pulse shape $a$, by a stationary phase argument, we have for $\pi \gamma T_p \gg T_p^{-1}$

$$\hat{s}(\omega) \simeq \frac{e^{-i\frac{\pi}{4}}}{2\sqrt{\gamma}} a \left( \frac{\omega - \omega_c}{2\pi \gamma T_p} \right) \exp \left( i\frac{(\omega - \omega_c)^2}{4\pi \gamma} \right), \tag{3}$$

which shows again that the bandwidth is $2\pi \gamma T_p$.

The antenna can be a point source, or a slotted waveguide [11], or a microstrip antenna [19]. In this paper, we will first carry out the analysis with a point source and then show how the results can be extended to the general antenna type. As we shall see in section 3.7, the beam antenna pattern plays the same role in the CINT imaging process and in the matched

filter process. The antenna moves along a straight trajectory, along the $x$-axis. The successive positions of the antenna are $\mathbf{x}_n = (x_n, 0, 0), n = 1, \ldots, N$, with $x_n = (n/N - 1/2)X_a$. The total length of the antenna trajectory is $X_a$. The antenna at $\mathbf{x}_n$ emits the signal $s(t - nT)$ and records the backscattered signal $R_n(t)$. A deramping is applied, that is, a multiplication by the opposite quadratic phase which recompresses the signal [5], so that we obtain the signals $S_n(t)$ defined by

$$S_n(t) = \exp[i\omega_c(t - nT - 2\tau_0) + i\pi\gamma(t - nT - 2\tau_0)^2]R_n(t), \tag{4}$$

where $\tau_0 = |\mathbf{x}_{N/2} - \mathbf{y}_0|/c_0, c_0$ is the reference background velocity, $\mathbf{y}_0$ is the center of the search area, and $\mathbf{x}_{N/2} = \mathbf{0}$ is the center of the antenna trajectory. The set of signals $S_n(t), n = 1, \ldots, N$, is the SAR set of data. We remark that the variable $t$ is sometimes referred to as the 'fast time' and the variable $n$ as the 'slow time' in the SAR literature. Moreover, centering with a fixed $\tau_0$ that does not depend on $n$ is sometimes referred to as strip map mode. Also note that deramping is typically done in hardware to lower the frequency band and enable analogue-to-digital conversion. Thus, only the signal after deramping is available for image formation.

Let us assume for a while that the antenna is a point source and that there is a single target in the medium, whose position is $\mathbf{y}_s$. This target acts a point scatterer. Using the Born approximation, the backscattered field measured at the antenna is [8]

$$R_n(t)|_{\text{single target}} = \frac{\omega_c^2}{2\pi} \int \hat{G}(\omega, \mathbf{x}_n, \mathbf{y}_s) v_s \hat{G}(\omega, \mathbf{y}_s, \mathbf{x}_n) \hat{s}(\omega) \, e^{-i\omega(t - nT)} \, d\omega$$

$$= \frac{\omega_c^2 v_s}{2\pi} \int \hat{G}(\omega, \mathbf{x}_n, \mathbf{y}_s)^2 \hat{s}(\omega) \, e^{-i\omega(t - nT)} \, d\omega,$$

where $v_s$ is the reflectivity of the scatterer and we have used the reciprocity identity $\hat{G}(\omega, \mathbf{x}, \mathbf{y}) = \hat{G}(\omega, \mathbf{y}, \mathbf{x})$. In a three-dimensional homogeneous medium with constant background velocity $c_0$, the Green's function is

$$\hat{G}(\omega, \mathbf{x}, \mathbf{y})|_{\text{homo}} = \frac{1}{4\pi|\mathbf{x} - \mathbf{y}|} e^{i\frac{\omega}{c_0}|\mathbf{x} - \mathbf{y}|}.$$

Therefore, in the case in which there is a single target at $\mathbf{y}_s$ and the medium is homogeneous, the recorded signal (after deramping) has the form

$$S_n(t)|_{\text{homo}} = \frac{\omega_c^2 v_s}{32\pi^2|\mathbf{y}_s - \mathbf{x}_n|^2} a\left(\frac{t - nT}{T_p} - 2\frac{|\mathbf{x}_n - \mathbf{y}_s|}{c_0 T_p}\right) \exp\left[2i\omega_c\left(\frac{|\mathbf{x}_n - \mathbf{y}_s|}{c_0} - \tau_0\right)\right]$$

$$\times \exp\left[4i\pi\gamma(t - nT - 2\tau_0)\left(\frac{|\mathbf{x}_n - \mathbf{y}_s|}{c_0} - \tau_0\right) - 4i\pi\gamma\left(\frac{|\mathbf{x}_n - \mathbf{y}_s|}{c_0} - \tau_0\right)^2\right],$$

and in the Fourier domain

$$\hat{S}_n(\omega)|_{\text{homo}} = \omega_c^2 v_s \hat{H}(\omega, \mathbf{x}_n, \mathbf{y}_s) \exp(i\omega(nT + 2\tau_0)), \tag{5}$$

where we have defined

$$\hat{H}(\omega, \mathbf{x}, \mathbf{y}) = \frac{T_p}{32\pi^2|\mathbf{y} - \mathbf{x}|^2} \hat{a}\left[T_p\left(4\pi\gamma\left(\frac{|\mathbf{x} - \mathbf{y}|}{c_0} - \tau_0\right) + \omega\right)\right] \exp\left[2i\omega_c\left(\frac{|\mathbf{x} - \mathbf{y}|}{c_0} - \tau_0\right)\right]$$

$$\times \exp\left[2i\omega\left(\frac{|\mathbf{x} - \mathbf{y}|}{c_0} - \tau_0\right) + 4i\pi\gamma\left(\frac{|\mathbf{x} - \mathbf{y}|}{c_0} - \tau_0\right)^2\right]. \tag{6}$$

Note that, as a function of $\mathbf{x}$, $\mathbf{y}$,

- the function $\hat{H}(\omega, \mathbf{x}, \mathbf{y})$ depends only on $|\mathbf{x} - \mathbf{y}|/c_0 - \tau_0$,
- its amplitude is concentrated at $|\mathbf{x} - \mathbf{y}| \simeq c_0(\tau_0 - \frac{\omega}{4\pi\gamma})$ (this property will give the range resolution as we will see below),
- since $\omega_c \gg \pi\gamma T_p$, the phase varies more rapidly than the amplitude (this property will give the azimuthal resolution as we will see below).

In general, the medium is not known and the usual SAR matched filter (or adjoint method) is the point spread function [8, 9]

$$
\begin{aligned}
I_n(\mathbf{y}) &= \int \overline{H}(t - nT - 2\tau_0, \mathbf{x}_n, \mathbf{y}) S_n(t) \, \mathrm{d}t \\
&= \frac{1}{2\pi} \int \overline{\hat{H}}(\omega, \mathbf{x}_n, \mathbf{y}) \exp(-\mathrm{i}\omega(nT + 2\tau_0)) \hat{S}_n(\omega) \, \mathrm{d}\omega,
\end{aligned}
\tag{7}
$$

where $\bar{\cdot}$ stands for complex conjugation. The point spread function matches the received signal $S_n$ against the synthetic signal $H$ that should be the one corresponding to the situation in which there is a point scatterer at the test point $\mathbf{y}$, and the medium is homogeneous with background velocity $c_0$. It is the optimal filter in the sense of providing the best signal-to-noise ratio in the presence of white noise [8, 9]. In SAR the point spread function is summed over $n$, which gives the ambiguity function of the SAR system

$$
\mathcal{I}(\mathbf{y}) = \left| \sum_{n=1}^{N} I_n(\mathbf{y}) \right|^2.
\tag{8}
$$

For the introduction of the CINT strategy, it is useful to expand the ambiguity function and to write it as

$$
\begin{aligned}
\mathcal{I}(\mathbf{y}) = \frac{1}{4\pi^2} \sum_{n,n'=1}^{N} \iint \overline{\hat{H}}(\omega, \mathbf{x}_n, \mathbf{y}) \hat{H}(\omega', \mathbf{x}_{n'}, \mathbf{y}) \\
\times \hat{S}_n(\omega) \overline{\hat{S}_{n'}(\omega')} \exp(\mathrm{i}\omega'(n'T + 2\tau_0) - \mathrm{i}\omega(nT + 2\tau_0)) \, \mathrm{d}\omega \, \mathrm{d}\omega'.
\end{aligned}
\tag{9}
$$

As we shall see in the following, this imaging functional produces very high-resolution images, and it is possible to quantify its performance in terms of resolution (subsection 3.3) and signal-to-noise ratios (subsections 3.4 and 3.5).

## 3. Coherent interferometric imaging

### 3.1. Coherent interferometric imaging strategy

The CINT strategy consists in restricting the double sum (over the antenna position) and the double integral (over the frequency) of the imaging functional (9) to those pairs which give a coherent contribution. Therefore, unnecessary incoherent contributions, that bring only noise, are not incorporated. If we introduce $X_d$ and $\Omega_d$ the cut-off parameters in space (along the antenna trajectory) and in frequency, then the CINT imaging functional is defined by

$$
\begin{aligned}
\mathcal{I}_{\mathrm{CINT}}(\mathbf{y}) = \frac{1}{4\pi^2} \sum_{|n-n'| \leqslant n_d/2} \iint_{|\omega-\omega'| \leqslant \Omega_d/2} \overline{\hat{H}}(\omega, \mathbf{x}_n, \mathbf{y}) \hat{H}(\omega', \mathbf{x}_{n'}, \mathbf{y}) \\
\times \hat{S}_n(\omega) \overline{\hat{S}_{n'}(\omega')} \exp(\mathrm{i}\omega'(n'T + 2\tau_0) - \mathrm{i}\omega(nT + 2\tau_0)) \, \mathrm{d}\omega \, \mathrm{d}\omega',
\end{aligned}
\tag{10}
$$

where $n_d = [N X_d / X_a]$. If $X_d$ is taken larger than the length of the antenna trajectory $X_a$ and $\Omega_d$ is taken larger than the source bandwidth $2\pi\gamma T_p$, then there is no truncation and we get the

matched filter imaging functional (9) of the SAR system. The resolution is then optimal, but the image can be very noisy as we shall see below. As $X_d$ and $\Omega_d$ are reduced, the resolution is reduced as well, but the noisy contributions are even more reduced, which results in an enhanced signal-to-noise ratio, as we will see below.

It is also possible to interpret the CINT imaging functional as the backpropagation of cross correlations over selected frequency-spatial windows [2]. Indeed, the expression $\overline{\hat{H}}(\omega, \mathbf{x}_n, \mathbf{y})\hat{S}_n(\omega)$ corresponds to the backpropagation of the signal $S_n$ (the complex conjugate over $\hat{H}$ corresponds to the time reversal operation). Therefore, in the usual point spread function (7), the recorded signals are backpropagated, and the matched filter functional is obtained by summing over $n$ and taking the square, which reads as the double sum and double integral (9). In the CINT functional (10), we restrict the sum over diagonal bands in $(\omega, \omega')$ and $(n, n')$. If these bands are larger than $T_p^{-1}$ and $N$, then we recover the matched filter imaging functional. If the frequency band is very small, so that we only retain the diagonal $\omega = \omega'$ and if we incorporate all spatial contributions of the synthetic array, then we obtain the interferometric function

$$\mathcal{I}_{\mathrm{INT}}(\mathbf{y}) = \frac{1}{4\pi^2} \sum_{n,n'=1}^{N} \int \overline{\hat{H}}(\omega, \mathbf{x}_n, \mathbf{y})\hat{H}(\omega, \mathbf{x}_{n'}, \mathbf{y})\hat{S}_n(\omega)\overline{\hat{S}_{n'}(\omega)} \exp(\mathrm{i}\omega(n'T - nT))\, \mathrm{d}\omega$$

$$= \frac{1}{2\pi} \sum_{n,n'=1}^{N} \int S_{n,\mathrm{back}}(t - nT)\overline{S_{n',\mathrm{back}}(t - n'T)}\, \mathrm{d}t, \tag{11}$$

where $S_{n,\mathrm{back}}(t)$ is the $n$th backpropagated recorded signal whose Fourier transform is $\hat{S}_{n,\mathrm{back}}(\omega) = \overline{\hat{H}}(\omega, \mathbf{x}_n, \mathbf{y})\hat{S}_n(\omega)$. This shows that $\mathcal{I}_{\mathrm{INT}}(\mathbf{y})$ is the cross correlation in time of the backpropagated recorded signals. The CINT strategy consists in restricting the double sum over $(n, n')$ in this formula to the terms that are coherent (i.e. the pairs $(n, n')$ such that $|n - n'| \leqslant n_d/2$), and to incorporate not only the diagonal $\omega' = \omega$ but also the diagonal band $|\omega' - \omega| \leqslant \Omega_d/2$ in which the frequency components are coherent.

The values of $\Omega_d$ and $X_d$ are *a priori* determined by the statistical properties of the random fluctuations of the background velocity of the medium, or the fluctuations of the antenna trajectory, or the statistical properties of the phenomenon responsible for the random fluctuations of the recorded signals. Ideally, the parameter $X_d$ should be the spatial correlation radius of the recorded signals along the antenna trajectory, and the parameter $\Omega_d$ should be their coherence bandwidth. It is possible to perform a detailed analysis of a particular model to determine these parameters, for instance, by studying the paraxial wave equation in a random medium [14, 15]. However, as shown in [2], it is better to select these parameters based on the quality of the image that is being formed from (10) and to use a feature preserving norm, such as the bounded variation (BV) norm or the entropy, to estimate the image quality. An adaptive procedure can be implemented, in which the values of $\Omega_d$ and $X_d$ are chosen in order to minimize the BV norm of the CINT imaging functional (10). This procedure results in an optimal compromise between resolution and smoothing [3].

### 3.2. A remark on the matched filter

In order to simplify the analysis, we shall here assume that the search point $\mathbf{y} = (x, y, z)$ and the target point $\mathbf{y}_s = (x_s, y_s, z_s)$ are close to the center of the search area $\mathbf{y}_0 = (x_0, y_0, z_0)$ and that the aperture is relatively small.

**Assumption 3.1.** $|\mathbf{y} - \mathbf{y}_0|, |\mathbf{y}_s - \mathbf{y}_0|, |x_s|, |x|, |x_0|, X_a \ll |\mathbf{y}_0|$

We can then expand

$$\frac{|\mathbf{x}_n - \mathbf{y}|}{c_0} - \tau_0 = \frac{\phi_n(\mathbf{r})}{2c_0|\mathbf{y}_0|} + \mathcal{O}\left(\frac{X_a}{c_0}\frac{X_a^2}{|\mathbf{y}_0|^2}\right),$$

$$\phi_n(\mathbf{r}) = (x - x_n)^2 - x_0^2 + |\mathbf{r} - \mathbf{r}_0|^2 + 2\mathbf{r}_0 \cdot (\mathbf{r} - \mathbf{r}_0) - \frac{(\mathbf{r}_0 \cdot (\mathbf{r} - \mathbf{r}_0))^2}{|\mathbf{r}_0|^2},$$

(12)

where $\mathbf{r} = (y, z)$, $\mathbf{r}_0 = (y_0, z_0)$, and $r = \sqrt{y^2 + z^2}$ is the range (i.e. the distance from the axis of the antenna trajectory to the test point $\mathbf{y}$). In the context of CINT it is of interest to examine the support in frequency of the product $\overline{\hat{H}(\omega, \mathbf{x}_n, \mathbf{y})}\hat{H}(\omega', \mathbf{x}_n, \mathbf{y})$. Note that for the chirp bandwidth $2\pi\gamma T_p$ we can associate the chirp wavelength

$$\lambda_{ch} = \frac{c_0}{\gamma T_p},$$

and the associated Fresnel number satisfies.

**Assumption 3.2.** The Fresnel number $N_a = X_a^2 / (\lambda_{ch}|\mathbf{y}_0|)$ is smaller than one or of order one.

In this regime the quantity $X_a^3 / (\lambda_{ch}|\mathbf{y}_0|^2)$ is much smaller than one and the function $\hat{H}(\omega, \mathbf{x}_n, \mathbf{y})$ given by (6) is non-zero only in the frequency range for $\omega$ such that

$$\left|\frac{2\pi\gamma\phi_n(\mathbf{r})}{c_0|\mathbf{y}_0|} + \omega\right| < \frac{1}{T_p}.$$

Therefore, the product $\overline{\hat{H}(\omega, \mathbf{x}_n, \mathbf{y})}\hat{H}(\omega', \mathbf{x}_{n'}, \mathbf{y})$ is not zero only if

$$\left|\frac{2\pi\gamma\phi_n(\mathbf{r})}{c_0|\mathbf{y}_0|} + \omega\right| < \frac{1}{T_p} \qquad \text{and} \qquad \left|\frac{2\pi\gamma\phi_{n'}(\mathbf{r})}{c_0|\mathbf{y}_0|} + \omega'\right| < \frac{1}{T_p}.$$

This shows that only the pairs of frequencies $(\omega, \omega')$ close to the diagonal $|\omega - \omega'| \leqslant \Omega_a$ contribute to the expression (9) of the ambiguity function and in the functional (10) of the CINT method, where $\Omega_a$ is defined by

$$\Omega_a = \frac{2 + 6\pi N_a}{T_p},$$

(13)

which is of order $T_p^{-1}$ by assumption 3.2. This implies that CINT in frequency is usually not useful, unless the coherence bandwidth of the medium is smaller than $\Omega_a$ which is very small (remember that the source bandwidth is $2\pi\gamma T_p \gg T_p^{-1}$). The matched filter for SAR with a chirped source is already in a CINT formulation in the frequency domain, in the sense that the integral over $(\omega, \omega')$ is naturally restricted to the diagonal $|\omega - \omega'| \leqslant \Omega_a$. The main reason for this is that a strong chirped source establishes a strong connection between time and frequency. Indeed, at a given time, the spectrum is concentrated around an instantaneous frequency, as can be shown by a stationary phase argument [8]. As a result, only the small frequency band around the instantaneous frequency corresponding to the correct travel time does contribute.

To summarize:

– The restriction $|\omega - \omega'| \leqslant \Omega_d/2$ in the CINT imaging functional (10) is effective only if $\Omega_d < 2\Omega_a$, otherwise it does not play any role.
– If $\Omega_d$ is larger than $2\Omega_a$, then we get that the CINT imaging functional takes the form

$$\mathcal{I}_{\text{CINT}}(\mathbf{y}) = \sum_{|n-n'|\leqslant n_d/2} I_n(\mathbf{y})\overline{I_{n'}(\mathbf{y})}.$$

– The restriction $|\omega - \omega'| \leqslant \Omega_d/2$ can be useful if the coherence bandwidth of the received signals is very small, i.e. smaller than $2\Omega_a$.

### 3.3. Range and azimuthal resolution

The resolution analysis for the ambiguity function (8) can be found in [8, 10], for instance. Here we revisit the arguments for the resolution analysis of the CINT imaging functional when the source is the chirped pulse (1), the medium is homogeneous, and there is a single point target located at $\mathbf{y}_s$. Under these conditions the recorded signal is given by (5), and the CINT imaging functional is

$$
\mathcal{I}_{\mathrm{CINT}}(\mathbf{y}) = \frac{|v_s|^2 \omega_c^4}{4\pi^2} \sum_{|n-n'| \leqslant n_d/2} \iint_{|\omega-\omega'| \leqslant \Omega_d/2} \overline{\hat{H}}(\omega, \mathbf{x}_n, \mathbf{y}) \hat{H}(\omega', \mathbf{x}_{n'}, \mathbf{y})
$$
$$
\times \hat{H}(\omega, \mathbf{x}_n, \mathbf{y}_s) \overline{\hat{H}}(\omega', \mathbf{x}_{n'}, \mathbf{y}_s) \, \mathrm{d}\omega \, \mathrm{d}\omega'.
$$

In order to get simple explicit characterizations for the resolution we make as before the assumptions 2.1, 3.1 and 3.2. In addition, in order to separate azimuthal and range resolution aspects we assume that $\mathbf{y}_0, \mathbf{y}$ and $\mathbf{y}_s$ lie in a plane through the antenna trajectory and with $\mathbf{y}_0 = (0, y_0, z_0)$. That is, labeling the range by $\mathbf{r} = (y, z)$ and $r = \sqrt{y^2 + z^2}$ (and similarly for $\mathbf{y}_0$ and $\mathbf{y}_s$), we assume

**Assumption 3.3.** $\mathbf{y}_0 = (0, \mathbf{e}_r r_0), \quad \mathbf{y} = (x, \mathbf{e}_r r), \quad \mathbf{y}_s = (x_s, \mathbf{e}_r r_s),$ where $\mathbf{e}_r$ is a two-dimensional unit vector.

By using (6) and assumptions 2.1, 3.1–3.3 and by keeping only the leading-order terms we get

$$
\overline{\hat{H}}(\omega, \mathbf{x}_n, \mathbf{y}) \hat{H}(\omega, \mathbf{x}_n, \mathbf{y}_s) \hat{H}(\omega', \mathbf{x}_{n'}, \mathbf{y}) \overline{\hat{H}}(\omega', \mathbf{x}_{n'}, \mathbf{y}_s)
$$
$$
= \frac{T_p^4}{2^{20} \pi^8 |\mathbf{y}_0|^8} \overline{\hat{a}} \left[ T_P \left( \frac{4\pi\gamma}{c_0} \left( (r - r_0) + \frac{(x - x_n)^2}{2|\mathbf{y}_0|} \right) + \omega \right) \right]
$$
$$
\times \hat{a} \left[ T_P \left( \frac{4\pi\gamma}{c_0} \left( (r_s - r_0) + \frac{(x_s - x_n)^2}{2|\mathbf{y}_0|} \right) + \omega \right) \right]
$$
$$
\times \hat{a} \left[ T_P \left( \frac{4\pi\gamma}{c_0} \left( (r - r_0) + \frac{(x - x_{n'})^2}{2|\mathbf{y}_0|} \right) + \omega' \right) \right]
$$
$$
\times \overline{\hat{a}} \left[ T_P \left( \frac{4\pi\gamma}{c_0} \left( (r_s - r_0) + \frac{(x_s - x_{n'})^2}{2|\mathbf{y}_0|} \right) + \omega' \right) \right]
$$
$$
\times \exp \left[ \mathrm{i} \frac{2\omega_c}{c_0 |\mathbf{y}_0|} (x_n - x_{n'})(x - x_s) \right]. \tag{14}
$$

Note first that the first terms in this expression (involving $\hat{a}$) give the range resolution since their common support is very small and forces $r$ to be close to $r_s$.

Note second that the last term in (14) gives the azimuthal resolution, after carrying out the summation over $n, n'$. We assume that $n_d = [X_d N / X_a]$ is always much larger than one in order to use the continuous approximation

$$
\sum_{|n-n'| \leqslant \frac{n_d}{2}} \exp \left[ \mathrm{i} \frac{2\omega_c}{c_0 |\mathbf{y}_0|} (x_n - x_{n'})(x - x_s) \right]
$$
$$
\sim \iint_{|\xi| \leqslant \frac{X_a}{2}, |\xi'| \leqslant \frac{X_a}{2}, |\xi-\xi'| \leqslant \frac{X_d}{2}} \exp \left[ \mathrm{i} \frac{2\omega_c}{c_0 |\mathbf{y}_0|} (\xi - \xi')(x - x_s) \right] \mathrm{d}\xi \, \mathrm{d}\xi',
$$

with

$$
X_d = n_d \Delta x, \qquad \Delta x = x_2 - x_1.
$$

This assumption simplifies the computation but the analysis could be extended by using summation formulae for exponential terms.

It is possible to distinguish four regimes, which are determined by the normalized quantities $\Omega_d/\Omega_a$ and $X_d/X_a$. We give here the asymptotic expressions of the CINT function imaging when these parameters are, each, either much smaller than one or larger than two.

– If $\Omega_d$ is larger than $2\Omega_a$ and $X_d$ is larger than $2X_a$, then the result of the matched filter imaging functional is recovered:

$$\mathcal{I}_{\text{CINT}}(\mathbf{y}) = I_0 F\left(\frac{4\pi\gamma T_p}{c_0}(r - r_s)\right)\text{sinc}^2\left(\frac{\omega_c X_a}{c_0|\mathbf{y}_0|}(x_s - x)\right), \tag{15}$$

where $\text{sinc}(x) = \sin(x)/x$ and

$$I_0 = \frac{|v_s|^2\omega_c^4 T_p^2 N^2}{2^{22}\pi^{10}|\mathbf{y}_0|^8},$$

$$F(r) = \left|\int \bar{\hat{a}}(r + u)\hat{a}(u)\,\mathrm{d}u\right|^2 = 4\pi^2\left|\int |a(s)|^2\mathrm{e}^{\mathrm{i}rs}\,\mathrm{d}s\right|^2.$$

This configuration gives the optimal range and azimuthal resolutions

$$\Delta r = \frac{c_0}{4\gamma T_p} \qquad \text{and} \qquad \Delta x = \frac{\pi c_0|\mathbf{y}_0|}{\omega_c X_a} = \frac{\lambda_c|\mathbf{y}_0|}{2X_a}.$$

– If $\Omega_d$ is larger than $2\Omega_a$ and $X_d$ is much smaller than $X_a$, then the CINT imaging functional is proportional to

$$\mathcal{I}_{\text{CINT}}(\mathbf{y}) = I_0\frac{X_d}{X_a}F\left(\frac{4\pi\gamma T_p}{c_0}(r - r_s)\right)\text{sinc}\left(\frac{\omega_c X_d}{c_0|\mathbf{y}_0|}(x_s - x)\right). \tag{16}$$

The range resolution is not affected:

$$\Delta r = \frac{c_0}{4\gamma T_p},$$

while the azimuthal resolution is reduced compared to the matched filter functional

$$\Delta x = \frac{\pi c_0|\mathbf{y}_0|}{\omega_c X_d} = \frac{\lambda_c|\mathbf{y}_0|}{2X_d}.$$

– If $\Omega_d$ is much smaller than $\Omega_a$ and $X_d$ is much smaller than $X_a$, then the CINT imaging functional is proportional to

$$\mathcal{I}_{\text{CINT}}(\mathbf{y}) = I_0\frac{X_d}{X_a}\Omega_d T_p G\left(\frac{4\pi\gamma T_p}{c_0}(r - r_s)\right)\text{sinc}\left(\frac{\omega_c X_d}{c_0|\mathbf{y}_0|}(x_s - x)\right), \tag{17}$$

where

$$G(r) = \int |\hat{a}(r + u)|^2|\hat{a}(u)|^2\,\mathrm{d}u.$$

The range resolution is not affected up to a shape factor (see the discussion below).

– If $\Omega_d$ is much smaller than $\Omega_a$ and $X_d$ is larger than $2X_a$, then the CINT imaging functional is proportional to

$$\mathcal{I}_{\text{CINT}}(\mathbf{y}) = I_0\Omega_d T_p G\left(\frac{4\pi\gamma T_p}{c_0}(r - r_s)\right)\text{sinc}^2\left(\frac{\omega_c X_a}{c_0|\mathbf{y}_0|}(x_s - x)\right). \tag{18}$$

**Table 1.** Resolution of the CINT method for different values of $X_d$ in the absence of noise. Only the azimuthal resolution depends on $X_d$. The range resolution is always $c_0/(4\gamma T_p)$.

| $X_d$ | $X_d \ll X_a$ | $2X_a < X_d$ |
|---|---|---|
| Azimuthal resolution | $\dfrac{\lambda_c|\mathbf{y}_0|}{2X_d}$ | $\dfrac{\lambda_c|\mathbf{y}_0|}{2X_a}$ |

Thus, the resolution is not changed relative to the matched filter imaging functional.

*Conclusion on the azimuthal resolution (see table* 1*).* The azimuthal resolution is determined by $X_a$ if $X_d$ is larger than $X_a$ and by $X_d$ if $X_d$ is smaller than $X_a$. Therefore, when $X_d$ is smaller than $X_a$, the azimuthal resolution does not depend on the length of the antenna trajectory anymore. However, the parameter $X_a$ still plays a role in the signal-to-noise ratio, as we will see in the following subsection.

*Conclusion on the range resolution.* The range resolution is determined by the bandwidth $2\pi\gamma T_p$. The choice of $\Omega_d$ plays a marginal role in that the normalized function that gives the shape of the focal spot in the range direction goes from $F$ when $\Omega_d$ is larger than $\Omega_a$ to $G$ when $\Omega_d$ is smaller than $\Omega_a$. It turns out that the function $F$ can be broader or narrower than $G$, depending on the source pulse shape $a(s)$. Let us consider three different cases, in which the pulse shape functions $a(s)$ have the same maximum and the same $L^2$-norm (i.e. the same energy):

$$\text{case 1:} \quad \begin{cases} a(s) = \mathbf{1}_{[-1,1]}(s) \\ \hat{a}(u) = 2\mathrm{sinc}(u) \end{cases} \tag{19}$$

$$\text{case 2:} \quad \begin{cases} a(s) = \exp(-\pi s^2/8) \\ \hat{a}(u) = 2\sqrt{2}\exp(-2u^2/\pi) \end{cases} \tag{20}$$

$$\text{case 3:} \quad \begin{cases} a(s) = \dfrac{5}{3\pi^2|s|^{5/2}}\left[\pi\sqrt{15}|s|S_i\left(\dfrac{2\sqrt{15}|s|^{1/2}}{5}\right) - 5|s|^{1/2}\sin^2\left(\dfrac{3\pi s}{5}\right)\right] \\ \hat{a}(u) = 5\left(1 - \dfrac{\sqrt{5|u|}}{\sqrt{6\pi}}\right)^2\mathbf{1}_{(-6\pi/5,6\pi/5)}(u) \end{cases} \tag{21}$$

where $S_i(s) = \int_0^s \sin(\pi s'^2/2)\,\mathrm{d}s'$ is the Fresnel sinus integral.

In figure 1 we plot the pulse intensity profiles $s \rightarrow a(s)^2$ for these three cases and the corresponding functions $F$ and $G$ (normalized by their respective maxima). One can check that taking $\Omega_d$ smaller than $\Omega_a$ reduces the range resolution for case 1 (since $G$ is broader than $F$), does not affect the resolution for case 2 (since $G$ is proportional to $F$), and enhances the resolution for case 3 (since $G$ is narrower than $F$). This discussion is just the starting point of a more general question about optimal illumination, that should address the optimal form of the source pulse shape. This question will be addressed in a future work in more detail.

### 3.4. Noise reduction

We next illustrate in an explicit fashion the mechanism responsible for the noise reduction with CINT in the SAR configuration. Assume a simple model in which the recorded travel times are perturbed by an additive zero-mean random vector $\tau_n^{(r)}$. By keeping only the leading-order
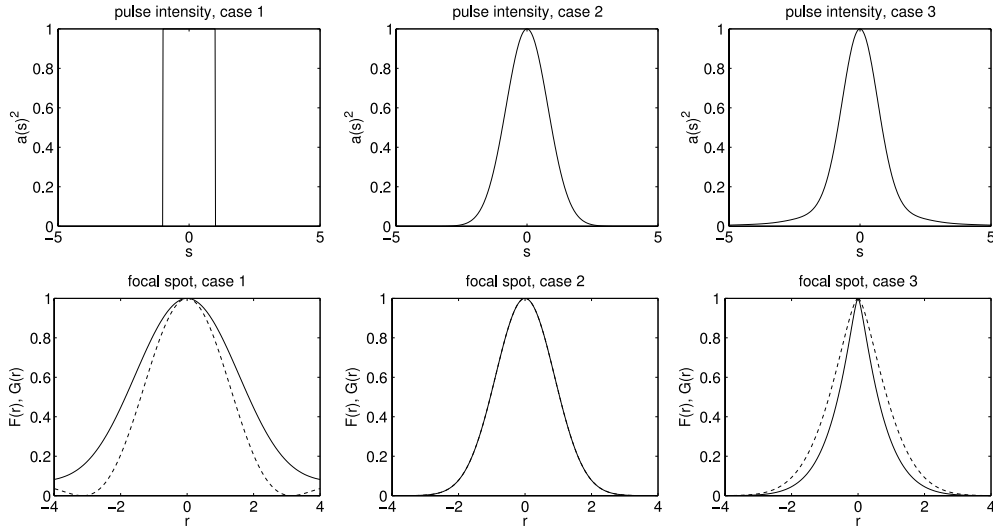
**Figure 1.** Pulse intensity profiles and focal spots (in the range direction) for the three cases described in (19)–(21). The solid lines plot the function $G$, the dashed lines plot the function $F$ (the two functions are equal in case 2).

terms, we have

$$
\begin{aligned}
\overline{\hat{H}}&(\omega, \mathbf{x}_n, \mathbf{y})\hat{S}_n(\omega)\hat{H}(\omega', \mathbf{x}_{n'}, \mathbf{y})\overline{\hat{S}_{n'}}(\omega') \exp(i\omega'(n'T + 2\tau_0) - i\omega(nT + 2\tau_0)) \\
&= \frac{T_p^4}{2^{20}\pi^8|\mathbf{y}_0|^8} \overline{\hat{a}}\left[ T_p\left( \frac{4\pi\gamma}{c_0}\left( (r - r_0) + \frac{(x - x_n)^2}{2|\mathbf{y}_0|}\right) + \omega\right)\right] \\
&\quad \times \hat{a}\left[ T_p\left( \frac{4\pi\gamma}{c_0}\left( (r_s - r_0) + \frac{(x_s - x_n)^2}{2|\mathbf{y}_0|}\right) + \omega\right)\right] \\
&\quad \times \hat{a}\left[ T_p\left( \frac{4\pi\gamma}{c_0}\left( (r - r_0) + \frac{(x - x_{n'})^2}{2|\mathbf{y}_0|}\right) + \omega'\right)\right] \\
&\quad \times \overline{\hat{a}}\left[ T_p\left( \frac{4\pi\gamma}{c_0}\left( (r_s - r_0) + \frac{(x_s - x_{n'})^2}{2|\mathbf{y}_0|}\right) + \omega'\right)\right] \\
&\quad \times \exp\left[ i\frac{2\omega_c}{c_0|\mathbf{y}_0|}(x_n - x_{n'})(x - x_s)\right] \exp\left( i\omega_c\left(\tau_n^{(r)} - \tau_{n'}^{(r)}\right)\right).
\end{aligned}
\tag{22}
$$

The last term in this expression is responsible for the reduction of the resolution and the enhancement of the fluctuations. If we assume that $\tau_n^{(r)}$ has Gaussian statistics and has Gaussian covariance function $\mathbb{E}\left[\tau_n^{(r)}\tau_{n'}^{(r)}\right] = \sigma_t^2 \exp\left(-(x_n - x_{n'})^2/l_c^2\right)$, then

$$
\mathbb{E}\left[ \exp\left( i\omega_c\left(\tau_n^{(r)} - \tau_{n'}^{(r)}\right)\right)\right] = \exp\left[ -\omega_c^2\sigma_t^2\left( 1 - \exp\left( -\frac{(x_n - x_{n'})^2}{l_c^2}\right)\right)\right].
\tag{23}
$$

If $\sigma_t\omega_c \gg 1$, then

$$
\mathbb{E}\left[ \exp\left( i\omega_c\left(\tau_n^{(r)} - \tau_{n'}^{(r)}\right)\right)\right] \simeq \exp\left( -\frac{\omega_c^2\sigma_t^2}{l_c^2}(x_n - x_{n'})^2\right),
\tag{24}
$$

which allows us to identify the correlation radius $X_c$ along the antenna trajectory:

$$
X_c = \frac{l_c}{\omega_c\sigma_t}.
\tag{25}
$$

Note that the Gaussian form of (24) is general and can be obtained from any form of the covariance function $\mathbb{E}\big[\tau_n^{(r)}\tau_{n'}^{(r)}\big]$, as long as it is at least twice differentiable at zero. We can then compute the first moments of the ambiguity function. If we assume that the correlation radius $X_c$ is smaller than the total length of the antenna trajectory, but larger than the distance between two successive positions of the antenna, i.e. $X_a/N \ll X_c \ll X_a$, then we obtain

$$\mathbb{E}[\mathcal{I}(\mathbf{y})] = I_0 \frac{\sqrt{\pi} X_c}{X_a} F\left(\frac{4\pi\gamma T_p}{c_0}(r - r_s)\right) \exp\left(-\left(\frac{\omega_c X_c}{c_0|\mathbf{y}_0|}(x - x_s)\right)^2\right), \quad (26)$$

which shows that the azimuthal resolution has been reduced to $\lambda_c|\mathbf{y}_0|/(2X_c)$. The covariance function of the ambiguity function is

$$\mathbb{E}[\mathcal{I}(\mathbf{y})\mathcal{I}(\mathbf{y}')] - \mathbb{E}[\mathcal{I}(\mathbf{y})]\mathbb{E}[\mathcal{I}(\mathbf{y}')] = I_0^2 \frac{\pi X_c^2}{X_a^2} F\left(\frac{4\pi\gamma T_p}{c_0}(r - r_s)\right) F\left(\frac{4\pi\gamma T_p}{c_0}(r' - r_s)\right)$$

$$\times \exp\left(-2\left(\frac{\omega_c X_c}{c_0|\mathbf{y}_0|}\left(\frac{x + x'}{2} - x_s\right)\right)^2\right) \text{sinc}^2\left(\frac{\omega_c X_a}{c_0|\mathbf{y}_0|}(x - x')\right), \quad (27)$$

which shows (for $\mathbf{y} = \mathbf{y}'$) that the fluctuations are strong, since the variance is equal to the square of the first moment and the signal-to-noise ratio is

$$\frac{\mathbb{E}^2[\mathcal{I}(\mathbf{y})]}{\text{Var}(\mathcal{I}(\mathbf{y}))} \overset{X_c \ll X_a}{\cong} 1. \quad (28)$$

If, additionally, there is additive noise or another type of external noise, then it will be very difficult to distinguish the coherent (mean) contribution. Moreover, the incoherent fluctuations are rapidly varying since the correlation radius is $\lambda_c|\mathbf{y}_0|/(2X_a)$. These fluctuations come from the contributions of the off-diagonal terms in (10) for which $|x_n - x_{n'}| \gg X_c$. These terms do not bring any coherent contribution, that is why the azimuthal resolution is limited to $\lambda_c|\mathbf{y}_0|/(2X_c)$. However, they bring incoherent contributions which enhance the noise.

Let us now discuss the CINT functional in the configuration $\Omega_d > 2\Omega_a$. The CINT functional is equivalent to the matched filter imaging functional if $X_d$ is larger than $2X_a$. If $X_d$ is much smaller than $X_a$ but larger than $X_c$, then we find that the first moment of the CINT functional is still the same as that of the matched filter functional

$$\mathbb{E}[\mathcal{I}_{\text{CINT}}(\mathbf{y})] = I_0 \frac{\sqrt{\pi} X_c}{X_a} F\left(\frac{4\pi\gamma T_p}{c_0}(r - r_s)\right) \exp\left(-\left(\frac{\omega_c X_c}{c_0|\mathbf{y}_0|}(x - x_s)\right)^2\right), \quad (29)$$

but the covariance function is different:

$$\mathbb{E}[\mathcal{I}_{\text{CINT}}(\mathbf{y})\mathcal{I}_{\text{CINT}}(\mathbf{y}')] - \mathbb{E}[\mathcal{I}_{\text{CINT}}(\mathbf{y})]\mathbb{E}[\mathcal{I}_{\text{CINT}}(\mathbf{y}')]$$

$$= I_0^2 \frac{\pi X_c^2 X_d}{X_a^3} F\left(\frac{4\pi\gamma T_p}{c_0}(r - r_s)\right) F\left(\frac{4\pi\gamma T_p}{c_0}(r' - r_s)\right)$$

$$\times \exp\left(-2\left(\frac{\omega_c X_c}{c_0|\mathbf{y}_0|}\left(\frac{x + x'}{2} - x_s\right)\right)^2\right) \text{sinc}\left(\frac{\omega_c X_d}{c_0|\mathbf{y}_0|}(x - x')\right). \quad (30)$$

This shows that the azimuthal resolution is still $\lambda_c|\mathbf{y}_0|/(2X_c)$ while the signal-to-noise ratio increases as $\sqrt{X_a}/\sqrt{X_d}$, as $X_d$ decays:

$$\frac{\mathbb{E}[\mathcal{I}_{\text{CINT}}(\mathbf{y})]}{\text{Var}(\mathcal{I}_{\text{CINT}}(\mathbf{y}))^{1/2}} \overset{X_c \ll X_d \ll X_a}{=} \frac{\sqrt{X_a}}{\sqrt{X_d}}. \quad (31)$$

The reason why the signal-to-noise ratio increases is that the incoherent terms (those for which $|x_n - x_{n'}| \gg X_c$) contribute less and less to the CINT imaging functional when $X_d$ decays.

**Table 2.** The resolution and signal-to-noise ratio of the CINT method for different values of $X_d$ in the case of a random perturbation of the recorded travel times of the form (23). The matched filter case is the same as the CINT case with $X_d > 2X_a$. The range resolution is always $c_0/(4\gamma T_p)$.

| $X_d$ | $X_d \ll X_c$ | $X_c \ll X_d \ll X_a$ | $2X_a < X_d$ |
|---|---|---|---|
| Azimuthal resolution | $\dfrac{\lambda_c|\mathbf{y}_0|}{2X_d}$ | $\dfrac{\lambda_c|\mathbf{y}_0|}{2X_c}$ | $\dfrac{\lambda_c|\mathbf{y}_0|}{2X_c}$ |
| SNR ratio | $\dfrac{\sqrt[4]{2}\sqrt{X_a}}{\sqrt[4]{\pi}\sqrt{X_c}}$ | $\dfrac{\sqrt{X_a}}{\sqrt{X_d}}$ | 1 |

Moreover, these incoherent terms do not contribute to the coherent image, so that the resolution is not affected by the decay of $X_d$, as long as it is larger than $X_c$.

Finally, if $X_d$ is smaller than $X_c$, then we find that

$$\mathbb{E}[\mathcal{I}_{\text{CINT}}(\mathbf{y})] = I_0 \frac{X_d}{X_a} F\left(\frac{4\pi\gamma T_p}{c_0}(r - r_s)\right) \text{sinc}\left(\frac{\omega_c X_d}{c_0|\mathbf{y}_0|}(x_s - x)\right), \tag{32}$$

while the covariance function is

$$\mathbb{E}[\mathcal{I}_{\text{CINT}}(\mathbf{y})\mathcal{I}_{\text{CINT}}(\mathbf{y}')] - \mathbb{E}[\mathcal{I}_{\text{CINT}}(\mathbf{y})]\mathbb{E}[\mathcal{I}_{\text{CINT}}(\mathbf{y}')] = I_0^2 \frac{\sqrt{\pi}X_d^2 X_c}{\sqrt{2}X_a^3} F\left(\frac{4\pi\gamma T_p}{c_0}(r - r_s)\right)$$

$$\times F\left(\frac{4\pi\gamma T_p}{c_0}(r' - r_s)\right) \text{sinc}\left(\frac{\omega_c X_d}{c_0|\mathbf{y}_0|}(x - x_s)\right) \text{sinc}\left(\frac{\omega_c X_d}{c_0|\mathbf{y}_0|}(x' - x_s)\right)$$

$$= \frac{\sqrt{\pi}X_c}{\sqrt{2}X_a} \mathbb{E}[\mathcal{I}_{\text{CINT}}(\mathbf{y})]\mathbb{E}[\mathcal{I}_{\text{CINT}}(\mathbf{y}')]. \tag{33}$$

Therefore, when $X_d/X_c$ decays, the resolution becomes poorer, of the order of $\lambda_c|\mathbf{y}_0|/(2X_d)$, while the signal-to-noise ratio saturates to a value proportional to $\sqrt{X_a}/\sqrt{X_c}$:

$$\frac{\mathbb{E}[\mathcal{I}_{\text{CINT}}(\mathbf{y})]}{\text{Var}(\mathcal{I}_{\text{CINT}}(\mathbf{y}))^{1/2}} \overset{X_d \ll X_c}{=} \frac{\sqrt[4]{2}\sqrt{X_a}}{\sqrt[4]{\pi}\sqrt{X_c}}. \tag{34}$$

The reason why the signal-to-noise ratio saturates is that the incoherent terms (those for which $|x_n - x_{n'}| \gg X_c$) are all taken out of the CINT imaging functional when $X_d$ is smaller than $X_c$, and to reduce further $X_d$ does not improve anymore the deblurring, while it affects the resolution since coherent contributions are removed.

We can briefly revisit the previous results for the CINT functional imaging in the configuration $\Omega_d \ll \Omega_a$. We obtain the same expressions as (29)–(34) with $F(\cdot)$ replaced by $\Omega_d T_p G(\cdot)$. Therefore the SNR analysis gives a result that is independent on the choice of $\Omega_d$.

*Conclusion of the SNR analysis (see table* 2*).* By choosing $X_d$ of the order of $X_c$, we obtain the best compromise between resolution and noise reduction. As shown in [3] the exact value of $X_d$ should be chosen adaptively in order to minimize the BV norm of the CINT image functional.

### 3.5. Impact of an additive white noise

Assume now that the received signals consist of the superposition of the signals generated by the backscattering of one point target $\mathbf{y}_s$ and an additive Gaussian white noise $\tilde{W}_n(\omega)$ (white in $n$ and 'almost' white in $\omega$):

$$\mathbb{E}[\hat{W}_n(\omega)\overline{\hat{W}_{n'}(\omega')}] = \sigma^2 \frac{|v_s|^2 \omega_c^4 T_p^2}{2^{10}\pi^4|\mathbf{y}_0|^4} \hat{\phi}(T_p(\omega - \omega'))\delta_{nn'}. \tag{35}$$

The variance parameter $\sigma^2$ has been normalized so that it is dimensionless, and the additive white noise has the same units as the signals reflected from the target. With this normalization, the reciprocal $1/\sigma$ is the signal-to-noise ratio of the recorded signals. This model includes the case in which the received signals consist of the backscattering of the point target $\mathbf{y}_s$ and the backscattering from a large collection of small and random scatterers (see the following subsection).

In the presence of the additive white noise (35) the CINT imaging functional can be written as

$$\mathcal{I}_{\mathrm{CINT}}(\mathbf{y}) = \mathcal{I}_{\mathrm{CINT}}^{\mathrm{targ}}(\mathbf{y}) + \mathcal{I}_{\mathrm{CINT}}^{i}(\mathbf{y}) + \mathcal{I}_{\mathrm{CINT}}^{ii}(\mathbf{y}), \tag{36}$$

where $\mathcal{I}_{\mathrm{CINT}}^{\mathrm{targ}}(\mathbf{y})$ is the image produced by the target in absence of random scatterers, while $\mathcal{I}_{\mathrm{CINT}}^{i}(\mathbf{y})$ and $\mathcal{I}_{\mathrm{CINT}}^{ii}(\mathbf{y})$ are the random terms

$$\mathcal{I}_{\mathrm{CINT}}^{i}(\mathbf{y}) = \frac{\omega_c^2 v_s}{4\pi^2} \sum_{|n-n'|\leqslant n_d/2} \iint_{|\omega-\omega'|\leqslant \Omega_d/2} \overline{\hat{H}}(\omega, \mathbf{x}_n, \mathbf{y})\hat{H}(\omega', \mathbf{x}_{n'}, \mathbf{y})$$

$$\times [\hat{H}(\omega, \mathbf{x}_n, \mathbf{y}_s)\overline{\hat{W}_{n'}(\omega')} + \overline{\hat{H}}(\omega', \mathbf{x}_{n'}, \mathbf{y}_s)\hat{W}_n(\omega)] \, \mathrm{d}\omega \, \mathrm{d}\omega',$$

$$\mathcal{I}_{\mathrm{CINT}}^{ii}(\mathbf{y}) = \frac{1}{4\pi^2} \sum_{|n-n'|\leqslant n_d/2} \iint_{|\omega-\omega'|\leqslant \Omega_d/2} \overline{\hat{H}}(\omega, \mathbf{x}_n, \mathbf{y})\hat{H}(\omega', \mathbf{x}_{n'}, \mathbf{y})\hat{W}_n(\omega)\overline{\hat{W}_{n'}(\omega')} \, \mathrm{d}\omega \, \mathrm{d}\omega'.$$

The matched filter imaging functional $\mathcal{I}(\mathbf{y})$ can be expanded in the same way. In the following, we assume once again that $\omega_c \gg \pi \gamma T_p \gg T_p^{-1}$ and $\Omega_d > 2\Omega_a$.

Let us first examine the matched filter imaging functional (i.e. the case $X_d > 2X_a$). The coherent component due to the target is

$$\mathcal{I}^{\mathrm{targ}}(\mathbf{y}) = I_0 F\left(\frac{4\pi\gamma T_p}{c_0}(r - r_s)\right)\mathrm{sinc}^2\left(\frac{\omega_c X_a}{c_0|\mathbf{y}_0|}(x_s - x)\right). \tag{37}$$

The first random component is a zero-mean process and its covariance function is

$$\mathbb{E}[\mathcal{I}^{i}(\mathbf{y})\mathcal{I}^{i}(\mathbf{y}')] = \frac{2\sigma^2}{N} I_0^2 F^{\frac{1}{2}}\left(\frac{4\pi\gamma T_p}{c_0}(r - r_s)\right) F^{\frac{1}{2}}\left(\frac{4\pi\gamma T_p}{c_0}(r' - r_s)\right)$$

$$\times F_\phi^{\frac{1}{2}}\left(\frac{4\pi\gamma T_p}{c_0}(r - r')\right)\mathrm{sinc}\left(\frac{\omega_c X_a(x - x_s)}{c_0|\mathbf{y}_0|}\right)\mathrm{sinc}\left(\frac{\omega_c X_a(x' - x_s)}{c_0|\mathbf{y}_0|}\right), \tag{38}$$

where $F_\phi$ is a generalized version of $F$ (we have $F_\phi = F$ in the pure white noise case):

$$F_\phi(u) = \left|\iint \hat{a}(u + u')\overline{\hat{a}}(u'')\hat{\phi}(u' - u'') \, \mathrm{d}u' \, \mathrm{d}u''\right|^2.$$

The second random component has a non-zero mean given by

$$\mathbb{E}[\mathcal{I}^{ii}(\mathbf{y})] = \frac{\sigma^2}{N} I_0 F_\phi(0)^{\frac{1}{2}}, \tag{39}$$

and its covariance function is

$$\mathbb{E}[\mathcal{I}^{ii}(\mathbf{y})\mathcal{I}^{ii}(\mathbf{y}')] - \mathbb{E}[\mathcal{I}^{ii}(\mathbf{y})]\mathbb{E}[\mathcal{I}^{ii}(\mathbf{y}')] = \frac{\sigma^4}{N^2} \frac{X_d}{X_a} I_0^2 F_\phi\left(\frac{4\pi\gamma T_p}{c_0}(r - r')\right)$$

$$\times \mathrm{sinc}^2\left(\frac{\omega_c X_a(x - x')}{c_0|\mathbf{y}_0|}\right). \tag{40}$$

The two components $\mathcal{I}^{i}(\mathbf{y})$ and $\mathcal{I}^{ii}(\mathbf{y})$ are not independent but they are uncorrelated

$$\mathbb{E}[\mathcal{I}^{i}(\mathbf{y})\mathcal{I}^{ii}(\mathbf{y}')] = 0. \tag{41}$$

Let us assume now that $X_d \ll X_a$, which is the interesting CINT configuration. The coherent component due to the target is

$$\mathcal{I}_{\text{CINT}}^{\text{targ}}(\mathbf{y}) = \frac{X_d}{X_a} I_0 F\left(\frac{4\pi\gamma T_p}{c_0}(r - r_s)\right) \text{sinc}\left(\frac{\omega_c X_d}{c_0|\mathbf{y}_0|}(x_s - x)\right). \tag{42}$$

The first random component is a zero-mean process and its covariance function is

$$\mathbb{E}\left[\mathcal{I}_{\text{CINT}}^i(\mathbf{y})\mathcal{I}_{\text{CINT}}^i(\mathbf{y}')\right] = \frac{2\sigma^2}{N}\frac{X_d^2}{X_a^2}I_0^2 F^{\frac{1}{2}}\left(\frac{4\pi\gamma T_p}{c_0}(r - r_s)\right)F^{\frac{1}{2}}\left(\frac{4\pi\gamma T_p}{c_0}(r' - r_s)\right)$$

$$\times F_\phi^{\frac{1}{2}}\left(\frac{4\pi\gamma T_p}{c_0}(r - r')\right)\text{sinc}\left(\frac{\omega_c X_d(x - x_s)}{c_0|\mathbf{y}_0|}\right)\text{sinc}\left(\frac{\omega_c X_d(x' - x_s)}{c_0|\mathbf{y}_0|}\right). \tag{43}$$

The second random component has a non-zero mean given by

$$\mathbb{E}\left[\mathcal{I}_{\text{CINT}}^{ii}(\mathbf{y})\right] = \frac{\sigma^2}{N}I_0 F_\phi(0)^{\frac{1}{2}} \tag{44}$$

and its covariance function is

$$\mathbb{E}\left[\mathcal{I}_{\text{CINT}}^{ii}(\mathbf{y})\mathcal{I}_{\text{CINT}}^{ii}(\mathbf{y}')\right] - \mathbb{E}\left[\mathcal{I}_{\text{CINT}}^{ii}(\mathbf{y})\right]\mathbb{E}\left[\mathcal{I}_{\text{CINT}}^{ii}(\mathbf{y}')\right] = \frac{\sigma^4}{N^2}\frac{X_d}{X_a}I_0^2 F_\phi\left(\frac{4\pi\gamma T_p}{c_0}(r - r')\right)$$

$$\times \text{sinc}\left(\frac{\omega_c X_d(x - x')}{c_0|\mathbf{y}_0|}\right). \tag{45}$$

The two components $\mathcal{I}_{\text{CINT}}^i(\mathbf{y})$ and $\mathcal{I}_{\text{CINT}}^{ii}(\mathbf{y})$ are not independent but they are uncorrelated as in (41):

$$\mathbb{E}\left[\mathcal{I}_{\text{CINT}}^i(\mathbf{y})\mathcal{I}_{\text{CINT}}^{ii}(\mathbf{y}')\right] = 0. \tag{46}$$

The first random component $\mathcal{I}_{\text{CINT}}^i(\mathbf{y})$ is a zero-mean noise whose support is located in the neighborhood of the target $\mathbf{y}_s$. Its typical amplitude relative to the coherent contribution is $2^{1/2}\sigma N^{-1/2}$, which is independent of the cut-off parameter $X_d$. The same component is found in the matched filter imaging functional.

The second random component is distributed in the search space where its statistical distribution is stationary. It gives rise to a background value, whose typical amplitude relative to the coherent contribution is $\sigma^2 N^{-1}(X_a/X_d)$. It has also fluctuations whose standard deviation (relative to the coherent contribution) is $\sigma^2 N^{-1}(X_a/X_d)^{1/2}$. Note that the mean of this contribution increases as $X_a/X_d$, while the standard deviation increases as $(X_a/X_d)^{1/2}$. This shows that this random noise is more important for the CINT method than for the matched filter functional, and especially the constant background is more and more noticeable as the cut-off parameter $X_d$ is taken smaller and smaller. In order to obtain the best signal-to-noise ratio, one should take $X_d$ larger than $X_a$, that is, one should use the matched filter imaging functional rather than the CINT method. Therefore, the CINT imaging method is efficient to reduce the blurring due to noise with a spatial structure, but it should not be used when the blurring originates purely from an additive white noise.

We can revisit the previous results in the configuration $\Omega_d \ll \Omega_a$. We get

$$\mathcal{I}_{\text{CINT}}^{\text{targ}}(\mathbf{y}) = \frac{X_d}{X_a}(\Omega_d T_p)I_0 G\left(\frac{4\pi\gamma T_p}{c_0}(r - r_s)\right)\text{sinc}\left(\frac{\omega_c X_d}{c_0|\mathbf{y}_0|}(x_s - x)\right), \tag{47}$$

$$\mathbb{E}\left[\mathcal{I}_{\text{CINT}}^i(\mathbf{y})\mathcal{I}_{\text{CINT}}^i(\mathbf{y}')\right] = \frac{2\sigma^2}{N}\frac{X_d^2}{X_a^2}(\Omega_d T_p)^2 I_0^2 G_\phi\left(\frac{4\pi\gamma T_p}{c_0}(r - r_s), \frac{4\pi\gamma T_p}{c_0}(r' - r_s)\right)$$

$$\times \text{sinc}\left(\frac{\omega_c X_d(x - x_s)}{c_0|\mathbf{y}_0|}\right)\text{sinc}\left(\frac{\omega_c X_d(x' - x_s)}{c_0|\mathbf{y}_0|}\right), \tag{48}$$

**Table 3.** Signal-to-noise ratios in the presence of an additive noise of the form (35). The distinction $\Omega_d$ larger or smaller than $\Omega_a$ plays a role only in the pre-factors that depend on the source intensity profile $a$.

| SNR ratio | $X_d \ll X_a$ | $2X_a < X_d$ |
|---|---|---|
| $\Omega_d \ll \Omega_a$ | $\dfrac{G(0)}{\hat{\phi}(0)F(0)^{\frac{1}{2}}} \dfrac{X_d N}{X_a \sigma^2}$ | $\dfrac{G(0)}{\hat{\phi}(0)F(0)^{\frac{1}{2}}} \dfrac{N}{\sigma^2}$ |
| $\Omega_d > 2\Omega_a$ | $\dfrac{F(0)}{F_\phi(0)^{\frac{1}{2}}} \dfrac{X_d N}{X_a \sigma^2}$ | $\dfrac{F(0)}{F_\phi(0)^{\frac{1}{2}}} \dfrac{N}{\sigma^2}$ |

$$\mathbb{E}\big[\mathcal{I}^{ii}_{\mathrm{CINT}}(\mathbf{y})\big] = \frac{\sigma^2}{N}(\Omega_d T_p)I_0\hat{\phi}(0)F^{\frac{1}{2}}(0), \tag{49}$$

$$\mathbb{E}\big[\mathcal{I}^{ii}_{\mathrm{CINT}}(\mathbf{y})\mathcal{I}^{ii}_{\mathrm{CINT}}(\mathbf{y}')\big] - \mathbb{E}\big[\mathcal{I}^{ii}_{\mathrm{CINT}}(\mathbf{y})\big]\mathbb{E}\big[\mathcal{I}^{ii}_{\mathrm{CINT}}(\mathbf{y}')\big] = \frac{\sigma^4}{N^2}\frac{X_d}{X_a}(\Omega_d T_p)^2 I_0^2$$

$$\times \tilde{G}_\phi\left(\frac{4\pi\gamma T_p}{c_0}(r-r')\right)\mathrm{sinc}\left(\frac{\omega_c X_d(x-x')}{c_0|\mathbf{y}_0|}\right), \tag{50}$$

where

$$G_\phi(r,r') = \iint |\hat{a}(s+r)|^2|\hat{a}(s'+r')|^2\hat{a}(s)\overline{\hat{a}(s')}\hat{\phi}(s-s')\,\mathrm{d}s\,\mathrm{d}s',$$

$$\tilde{G}_\phi(r) = \iint |\hat{a}(s)|^2|\hat{a}(s'+r)|^2\hat{\phi}(s-s')\,\mathrm{d}s\,\mathrm{d}s'.$$

Therefore, changing the configuration so that $\Omega_d$ is smaller than $\Omega_a$:

- multiplies the first moments by $\Omega_d T_p$ and the second moments by $(\Omega_d T_p)^2$, which does not affect the resolution nor the signal-to-noise ratio,
- changes the shape functions $F$, $F_\phi$, which has a marginal effect on the resolution and on the signal-to-noise ratio. We have already shown in subsection 3.3 that the resolution can be enhanced or reduced depending on the source pulse intensity profile $a(s)$. The same remark holds true for the signal-to-noise ratio. Indeed, as shown in table 3, the pre-factor for the signal-to-noise ratio is $\frac{G(0)}{\hat{\phi}(0)F(0)^{\frac{1}{2}}}$ if $\Omega_d \ll \Omega_a$ and $\frac{F(0)}{F_\phi(0)^{\frac{1}{2}}}$ if $\Omega_d > 2\Omega_a$.

When the additive noise comes from the backscattering of a collection of small random scatterers (see the following subsection), then the function $\hat{\phi}$ is equal to $F^{1/2}$ and therefore:

- If $\Omega_d \ll \Omega_a$, then the pre-factor is $\dfrac{G(0)}{\hat{\phi}(0)F(0)^{\frac{1}{2}}} = \dfrac{\int |\hat{a}(u)|^4\,\mathrm{d}u}{\left(\int |\hat{a}(u)|^2\,\mathrm{d}u\right)^2}.$

- If $\Omega_d > 2\Omega_a$, then the pre-factor is $\dfrac{F(0)}{F_\phi(0)^{\frac{1}{2}}} = \dfrac{1}{2\pi}\dfrac{\left(\int |a(s)|^2\,\mathrm{d}s\right)^2}{\int |a(s)|^4\,\mathrm{d}s}.$

For the three examples described in (19)–(21) we obtain

- If $\Omega_d \ll \Omega_a$, then the pre-factor is $\dfrac{G(0)}{\hat{\phi}(0)F(0)^{\frac{1}{2}}} = \begin{cases} \frac{2}{3\pi} & \text{case 1} \\ \sqrt{2} & \text{case 2} \\ 0.66 & \text{case 3} \end{cases}$

- If $\Omega_d > 2\Omega_a$, then the pre-factor is $\dfrac{F(0)}{F_\phi(0)^{\frac{1}{2}}} = \begin{cases} \frac{1}{\pi} & \text{case 1} \\ \sqrt{2} & \text{case 2} \\ 0.50 & \text{case 3} \end{cases}$

Note that the pre-factor can be enhanced or reduced when going from $\Omega_d > 2\Omega_a$ to $\Omega_d \ll \Omega_a$, depending on the source intensity profile $a$. If we consider case 1, that is the one which is usually implemented in SAR systems, then the range resolution is degraded and the signal-to-noise ratio reduced when we go from $\Omega_d > 2\Omega_a$ to $\Omega_d \ll \Omega_a$.

### 3.6. An additive white noise model

It is possible to construct a simple model that gives a white noise of the form (35). If we assume that the medium contains a collection of small scatterers, then the incoherent contribution to the received signal (after deramping) is

$$\hat{W}_n(\omega) = \omega_c^2 \sum_j v_j \hat{H}(\omega, \mathbf{x}_n, \mathbf{y}_j) \exp(\mathrm{i}\omega(nT + \tau_0)), \tag{51}$$

where $v_j$ is the reflectivity of the $j$th scatterer and $\mathbf{y}_j$ is its position. When the antenna has some directionality, then the sum over $j$ is restricted to the scatterers located in the area illuminated by the antenna. Let us assume that the antenna beam pattern along the $x$-axis is a cone with angular aperture $\theta_{||}$ and with distribution $w_{||}(\theta/\theta_{||})$ along the axis perpendicular to the antenna trajectory and directed toward the search area, and with angular aperture $\theta_\perp$ and with distribution $w_\perp(\theta/\theta_\perp)$ perpendicular to this axis. If the collection of scatterers is dense and each scatterer is small, then the central limit theorem can be applied in the single-scattering approximation. We obtain that $\hat{W}_n$ has Gaussian statistics with zero-mean and autocorrelation function

$$\mathbb{E}[\hat{W}_n(\omega)\overline{\hat{W}_{n'}(\omega')}] = q^2 F^{\frac{1}{2}}(T_p(\omega - \omega')) \frac{\hat{w}_{||}\left(\frac{2\theta_{||}\omega_c}{c_0}(x_{n'} - x_n)\right)}{\hat{w}_{||}(0)} \exp\left(\mathrm{i}\frac{\omega_c}{c_0|\mathbf{y}_0|}\left(x_n^2 - x_{n'}^2\right)\right).$$

Here $q^2$ is given by

$$q^2 = \frac{\langle|v|^2\rangle\omega_c^4 T_p^2}{2^{10}\pi^4|\mathbf{y}_0|^4}\left[\mathcal{D}\frac{c_0}{4\pi\gamma T_p}|\mathbf{y}_0|^2\theta_{||}\theta_\perp\hat{w}_{||}(0)\hat{w}_\perp(0)\right],$$

where $\langle|v|^2\rangle$ is the mean squared reflectivity of the small scatterers and $\mathcal{D}$ is the density of scatterers per unit volume. In this expression, the square brackets give the number of scatterers that contribute to the noise in the recorded signals. If the distance between two successive positions of the antenna is larger than $2\pi\lambda_c/\theta_{||}$, then we get a white-noise model in $n$:

$$\mathbb{E}[\hat{W}_n(\omega)\overline{\hat{W}_{n'}(\omega')}] = \sigma^2 \frac{|v_s|^2\omega_c^4 T_p^2}{2^{10}\pi^4|\mathbf{y}_0|^4} F^{\frac{1}{2}}(T_p(\omega - \omega'))\delta_{nn'}, \tag{52}$$

which has the form (35) with

$$\sigma^2 = \frac{\langle|v|^2\rangle}{|v_s|^2}\left[\mathcal{D}\frac{c_0}{4\pi\gamma T_p}|\mathbf{y}_0|^2\theta_{||}\theta_\perp\hat{w}_{||}(0)\hat{w}_\perp(0)\right].$$

Note that, as the distance $|\mathbf{y}_0|$ increases, the parameter $\sigma^2$ increases as $|\mathbf{y}_0|^2$. This is due to the fact that more small scatterers contribute to the noise in the recorded signals when the antenna probes regions further away from the antenna.

### 3.7. Role of the antenna beam pattern

As pointed out in section 2, the antenna can be a point source, or a slotted waveguide, or a microstrip antenna. The antenna can then be modeled by a rectangular distribution of point sources [23], which lie in the $(xy)$ plane, whose length (along the $x$-axis) is $L$, and whose width

(along the $y$-axis) is $D$. When there is a single target at $\mathbf{y}_s$ and the medium is homogeneous, then the recorded signal has the form

$$S_n(t)|_{\text{homo}} = \frac{\omega_c^2 v_s w(\mathbf{y}_s - \mathbf{x}_n)}{16\pi^2 |\mathbf{y}_s - \mathbf{x}_n|^2} a\left(\frac{t - nT}{T_p} - 2\frac{|\mathbf{x}_n - \mathbf{y}_s|}{c_0 T_p}\right) \exp\left[2i\omega_c\left(\frac{|\mathbf{x}_n - \mathbf{y}_s|}{c_0} - \tau_0\right)\right]$$

$$\times \exp\left[4i\pi\gamma(t - nT - 2\tau_0)\left(\frac{|\mathbf{x}_n - \mathbf{y}_s|}{c_0} - \tau_0\right) - 4i\pi\gamma\left(\frac{|\mathbf{x}_n - \mathbf{y}_s|}{c_0} - \tau_0\right)^2\right].$$

The difference with the point-source antenna case is the presence of the function $w$, which is the antenna beam pattern. In the case of a point source, it is a constant. In the case of a rectangular distribution of point sources with length $L$ and width $D$, we have for $\mathbf{y} = (x, y, z)$ such that $|\mathbf{y}|$ is larger than $L$, $D$, $L^2/\lambda_c$ and $D^2/\lambda_c$ [8]:

$$w(\mathbf{y}) = LD\,\text{sinc}\left(\frac{\omega_c L}{2c_0}\frac{x}{|\mathbf{y}|}\right)\text{sinc}\left(\frac{\omega_c D}{2c_0}\frac{y}{|\mathbf{y}|}\right). \tag{53}$$

The role of the beam pattern is the same for the matched filter and for the CINT method, and it can be understood by noting that a reflected signal from the target can be recorded only if the target is in the footprint of the beam pattern. Consequently:

– The $x$-dependence of the beam pattern gives the upper bound for the length of the antenna path $X_a$. If $X_a$ is smaller than $2\lambda_c|\mathbf{y}_0|/L$, then the $x$-dependence of the beam pattern plays no role. If $X_a$ is larger than $2\lambda_c|\mathbf{y}_0|/L$, then only a piece of the trajectory, with length $2\lambda_c|\mathbf{y}_0|/L$, illuminates the target and plays a role. In this case, one should substitute $2\lambda_c|\mathbf{y}_0|/L$ for $X_a$ in the previous results.

– The $y$-dependence can be used to obtain a three-dimensional image. Indeed, with a point source as an antenna, we only get azimuthal and range resolutions, that is, information on the coordinates $x_s$ and $\sqrt{y_s^2 + z_s^2}$ of the target. Using the range estimate and the $y$-dependence of the beam pattern, one can distinguish between the coordinates $y_s$ and $z_s$. The $y$-dependence of the beam pattern shows that the angle between $y_s$ and $z_s$ can be estimated with the precision $\lambda_c/D$.

## 4. Numerical simulations

We consider an experimental configuration in which the antenna is on a rail system. The center of the search area is at $\mathbf{y}_0 = (0, y_0, 0)$ with $y_0 = 440$ m. The length of the antenna trajectory is $X_a = 11$ m. The pulse width is $T_p = 2\,10^{-6}$ s. The carrier frequency is $\omega_c = 2\pi 35.3\,10^9$ s$^{-1}$. The chirp parameter is $\gamma = 5\,10^{14}$ s$^{-2}$. The reference background velocity is $c_0 = 3\,10^8$ m s$^{-1}$. In this scaling, motivated by a specific SAR instrumentation, we have indeed

*Assumption* 2.1; $\omega_c \gg \pi\gamma T_p \gg T_p^{-1}$: $2.2\,10^{11} \gg 3.1\,10^9 \gg 5\,10^5$.

*Assumption* 3.1; $X_a \ll y_0$: $11 \ll 440$.

*Assumption* 3.2; $X_a^2/(\lambda_{\text{ch}}|\mathbf{y}_0|) = 0.3 < 1$.

*Assumption* 3.3; $\mathbf{e}_r = (1, 0)$.

The optimal range resolution is $c_0/(4\gamma T_p) \sim 0.1$ m and the optimal azimuthal resolution is $\lambda_c|\mathbf{y}_0|/(2X_a) \sim 0.2$ m.

The two target points have the same reflectivity and they are in the plane $z = 0$. We plot the imaging functionals in this plane, the images are normalized by their maximal values and plotted on a log scale. The numerical recorded signals are the homogeneous signals $\hat{H}(\omega, \mathbf{x}_n, \mathbf{y}_s)$ produced by two point targets and we assume that the recorded travel times are
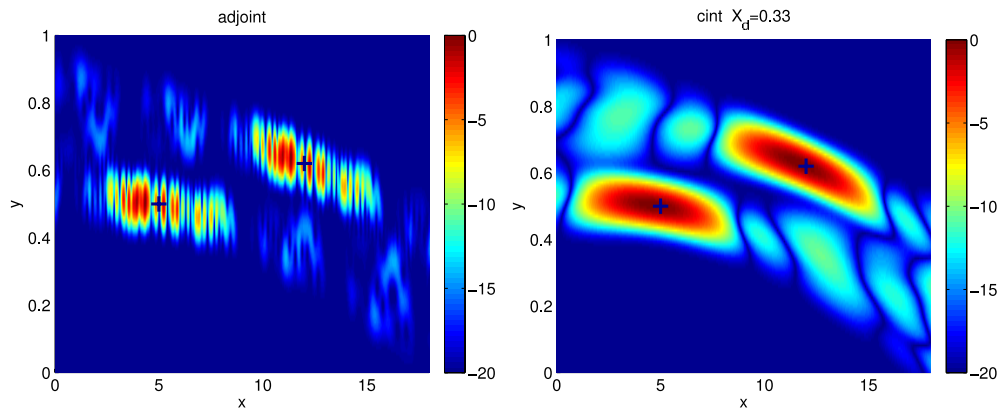
**Figure 2.** Standard imaging functional (adjoint or matched filter method) and CINT imaging functionals. The recorded travel times are randomly perturbed but there is no additive white noise. The crosses stand for the real locations of the two point targets. The coordinates $x$ and $y$ are in meter and the images are plotted in dB (i.e. $10 \log_{10}(\mathcal{I}/\max \mathcal{I})$).
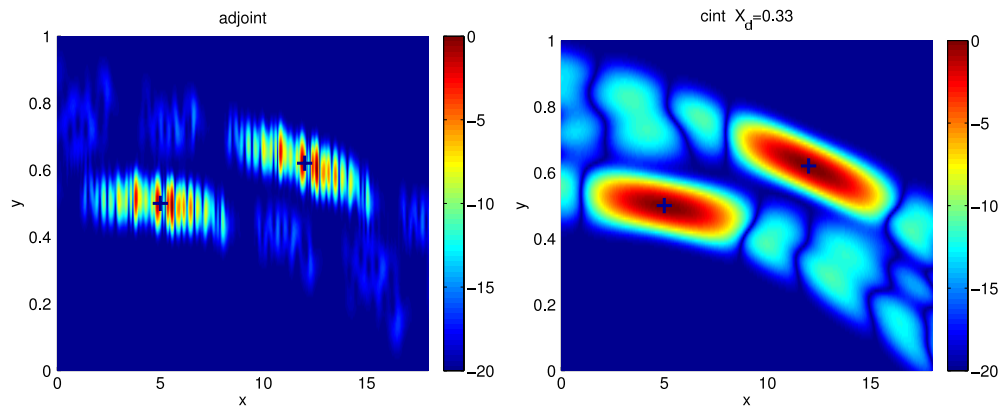


**Figure 3.** Same as in figure 2, but with a different realization of the perturbations.

perturbed by an additive Gaussian process. The standard deviation of this Gaussian process is $10^{-10}$ s, which corresponds to a travel distance of 0.03 m. The associated correlation radius of the observations on the antenna is $X_c = 0.4$ m. In figures 2 and 3 we assume the absence of any external additive noise, while in figures 4–6 we consider the presence of an additive Gaussian white noise whose amplitude is equivalent to the amplitude of the unperturbed signal (0 dB additive noise).

In figures 2 and 3 (no additive white noise) the image is very noisy for the matched filter imaging functional. As predicted by the theory (see the moments (26) and (27)), we observe around each target a structure with azimuthal size $\lambda_c |\mathbf{y}_0|/(2X_c)$ and with rapid fluctuations (in the azimuthal direction) with the correlation length $\lambda_c |\mathbf{y}_0|/(2X_a)$. The image obtained with the CINT method with the parameter $X_d = 0.33$ m (of the order of $X_c$) is much clearer and has the same resolution.

In figures 4–6 we can see the impact of an additive white noise. It should be noted that the additive white noise generates a clutter in the image whose azimuthal correlation length is
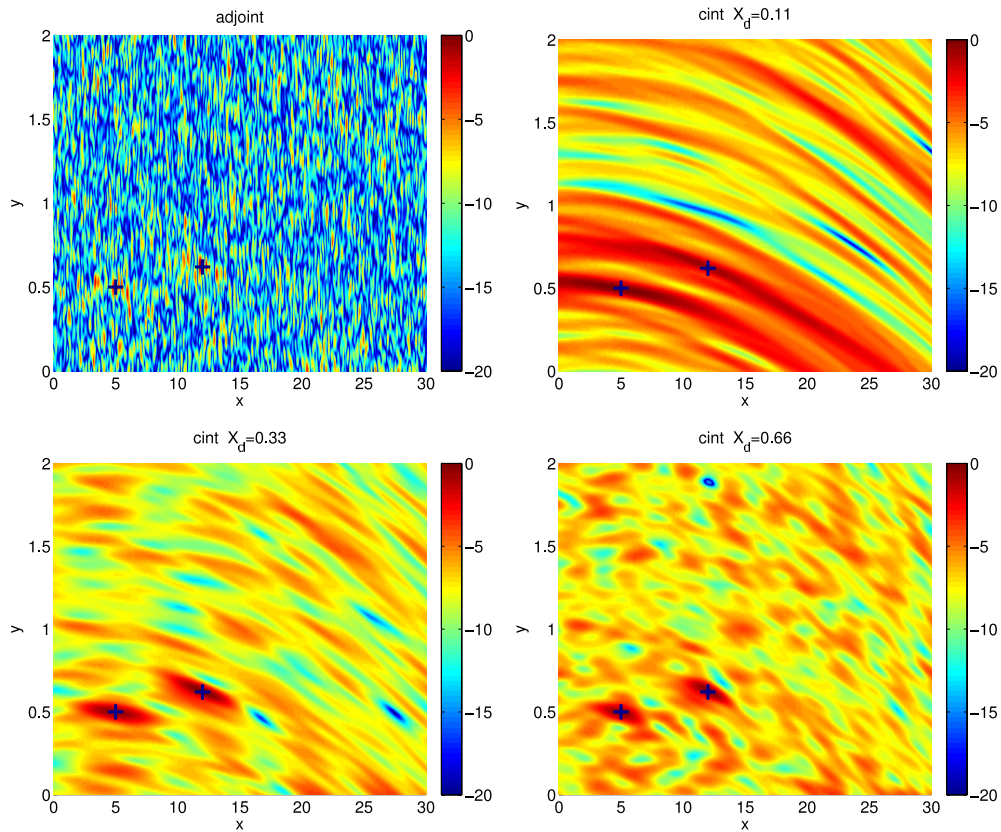
19

**Figure 4.** Standard imaging functional and CINT imaging functionals for different values of the cut-off parameter $X_d$ (in dB). The recorded travel times are randomly perturbed and an additive white noise has been added. The crosses stand for the real locations of the two point targets. Here the minimum of the imaging functional over the search window has been subtracted before normalization by the maximal value.

$\lambda_c |\mathbf{y}_0|/(2X_a)$, that is, of the same order as the correlation length of the fluctuations of the main structures associated with the targets. As a result, the target structures are now embedded in the clutter produced by the additive white noise and they are very difficult to identify. Furthermore, the images are not stable, in the sense that they change from one realization of the random perturbation to the other one (compare the top-left images in figures 4 and 5). In particular, the maximum of the imaging functional is a fluctuating quantity. The image produced by the CINT imaging functional with the parameter $X_d = 0.33$ m (of the order of $X_c$) has a reduced noise level and exhibits the same overall structures, which make it possible to identify the two targets. If the parameter $X_d$ is chosen larger than $X_c$, then the noise level is still high. If the parameter $X_d$ is chosen smaller than $X_c$, then the noise level is very low but resolution has been degraded. In figures 4 and 5 the minimum of the imaging functional is subtracted before normalization, which removes most of the background due to the additive white noise when $X_d$ is small. In figure 6 the minimum is not subtracted and one can see the constant background due to the additive white noise identified in the previous subsection 3.5, when $X_d$ is small. There is almost no background when $X_d = 0.66$ m or larger, so that the images are very similar with or without subtraction of the minimum for large $X_d$. Finally,
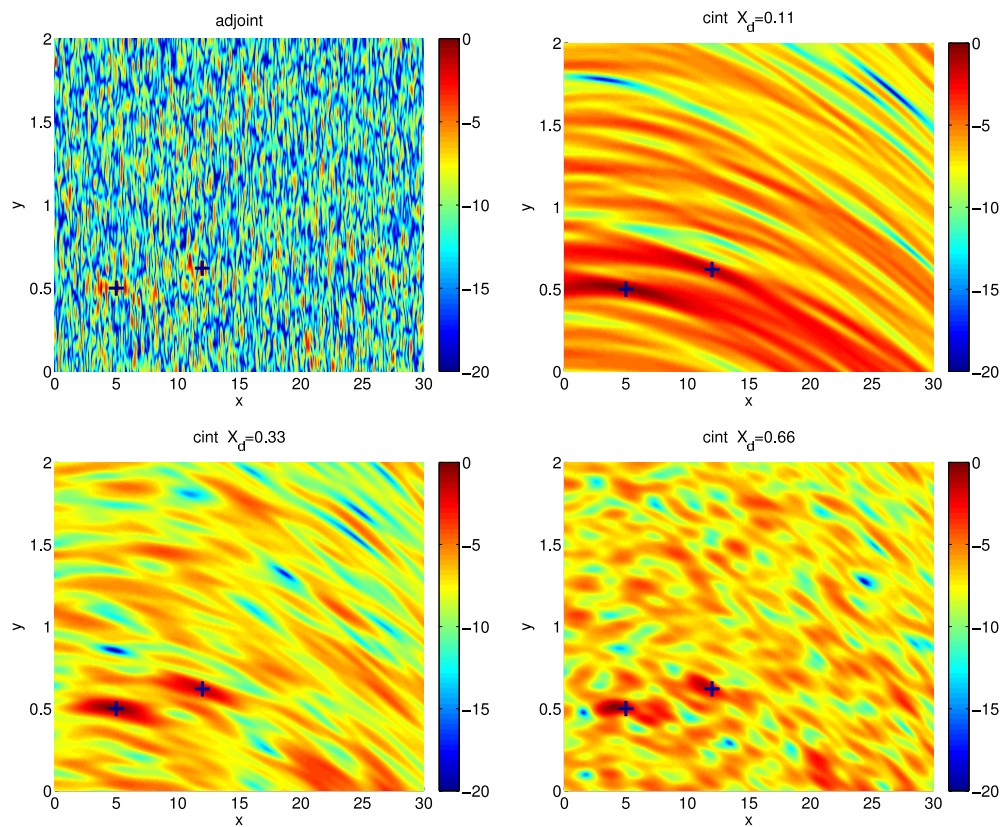
20

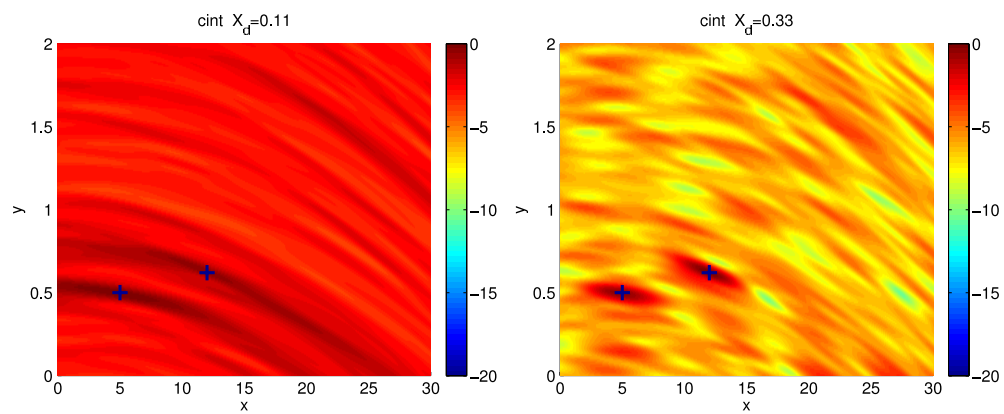**Figure 5.** Same as in figure 4 but for a different realization of the random fluctuations.



**Figure 6.** Same as in figure 4, but the minimum of the imaging functional has not been subtracted, which creates the background.

note that the CINT image is less fluctuating than that obtained by the matched filter ambiguity function, in the sense that the quality of the final image depends primarily on the statistics

of the random fluctuations, and not on the particular realizations (compare the bottom-left images in figures 4 and 5).

## 5. Conclusion

In this paper, we have shown that the CINT imaging method can enhance the signal-to-noise ratio dramatically, without affecting the resolution. It is efficient when the fluctuations of the recorded signals have a spatial correlation (along the antenna trajectory) that is larger than the distance between two successive positions of the antenna and smaller than the length of the antenna trajectory. However, it is not efficient to deal with a pure additive white noise, in the presence of which the matched filter processing should be used. We have discussed the advantages and the limitations of the CINT strategy in the SAR context. On the one hand, we have stressed that the SAR method based on the use of a strongly chirped source is already in a CINT configuration in the frequency domain. On the other hand, we have shown the benefit of the CINT operation in the spatial domain, by showing that statistically stable images can be obtained with a very reduced noise level. An optimal compromise between the signal-to-noise ratio and resolution can be achieved by a proper choice of the spatial cut-off parameter, which is of the order of the correlation radius of the fluctuations of the recorded signals along the antenna trajectory.

## Acknowledgments

## Appendix. Examples

The results of this paper are derived in the regime of separation of scales $\omega_c \gg \pi\gamma T_p \gg T_p^{-1}$. This is in fact the typical SAR regime. For instance:

- The parameters of the satellite ERS-1 are the following ones [16]. The carrier frequency is $\omega_c = 2\pi\,5.3\,10^9$ s$^{-1}$. The pulse duration is $T_p = 37.1\,10^{-6}$ s. The chirp parameter is $\gamma = 4.2\,10^{11}$ s$^{-2}$. As a result we have $\omega_c \gg \pi\gamma T_p \gg T_p^{-1}$ ($3.3\,10^{10} \gg 4.9\,10^7 \gg 2.7\,10^4$).
- An example of SAR design is given in [5, p. 76]: $\omega_c = 2\pi\,10^{10}$ s$^{-1}$, $T_p = 38.5\,10^{-6}$ s, and $\gamma = 4.8\,10^{12}$ s$^{-2}$. As a result we have $\omega_c \gg \pi\gamma T_p \gg T_p^{-1}$ ($6.3\,10^{10} \gg 5.8\,10^8 \gg 2.6\,10^4$).

## References

[1] Borcea L, Papanicolaou G and Tsogka C 2005 Interferometric array imaging in clutter *Inverse Problems* **21** 1419–60
[2] Borcea L, Papanicolaou G and Tsogka C 2006 Adaptive interferometric imaging in clutter and optimal illumination *Inverse Problems* **22** 1405–36
[3] Borcea L, Papanicolaou G and Tsogka C 2006 Coherent interferometric imaging *Geophysics* **71** S1165–75
[4] Borcea L, Papanicolaou G and Tsogka C 2006 Coherent interferometry in finely layered random media *SIAM Multiscale Model. Simul.* **5** 62–83
[5] Carrara W G, Goodman R S and Majewski R M 1995 *Spotlight Synthetic Aperture Radar* (Boston: Artech House)

[6]  Çetin M and Karl W C 2000 Superresolution and edge-preserving reconstruction of complex-valued synthetic aperture radar images *Proc. IEEE Int. Conf. on Image Processing (Vancouver, Canada)* vol 1 pp 701–4

[7]  Chan H L and Yea T S 2002 Noniterative quality phase-gradient autofocus (QPGA) algorithm for spotlight SAR imagery *IEEE Trans. Geosci. Remote Sens.* **36** 1531–9

[8]  Cheney M 2001 A mathematical tutorial on synthetic aperture radar *SIAM Rev.* **43** 301–12

[9]  Curlander J C and McDonough R N 1991 *Synthetic Aperture Radar* (New York: Wiley)

[10]  Cutrona L J 1990 Synthetic aperture radar *Radar Handbook* 2nd edn ed M Skolnik (New York: McGraw-Hill)

[11]  Derneryd A G, Petersson R N O and Ingvarson P 1994 Slotted waveguide antennas for remote sensing satellites *Proc. of the Progress in Electromagnetic Research Symp. (Nordwijk, The Netherlands)*

[12]  Eichel P H and Jakowatz C V Jr 1989 Phase-gradient algorithm as an optimal estimator of the phase derivative *Opt. Lett.* **14** 1101–3

[13]  Elachi C 1987 *Spaceborne Radar Remote Sensing* (New York: IEEE Press)

[14]  Fannjiang A C 2005 White-noise and geometrical optics limits of Wigner–Moyal equation for beam waves in turbulent media II. Two-frequency formulation *J. Stat. Phys.* **120** 543–86

[15]  Fannjiang A C and Yan M 2007 Multi-frequency imaging of multiple targets in Rician fading channels: stability and resolution *Inverse Problems* **23** 1801–19

[16]  Guyenne T D (ed) 1977 Engineering achievements of ERS-1 *European Space Agency SP-11197/III* (Noordwijk, The Netherlands: ESA Publications Division, ESTEC)

[17]  Koo V C, Lim T S and Chuah H T 2005 A comparison of autofocus algorithms for SAR imagery *Proc. of the Progress In Electromagnetics Research Symp. (Hangzhou, China), PIERS Online* **1** 16–9

[18]  Nolan C J and Cheney M 2002 Synthetic aperture inversion *Inverse Problems* **18** 221–35

[19]  Petersson R N O, Derneryd A G and Ingvarson P 1994 Microstrip antennas for remote sensing satellites *Proc. of the Progress in Electromagnetic Research Symp. (Nordwijk, The Netherlands)*

[20]  van Rossum W L, Otten M P G and van Bree R J P 2006 Extended PGA for Range Migration Algorithms *IEEE Trans. Aero. Electron. Syst.* **42** 478–88

[21]  Wahl D E, Eichel P H, Ghiglia D C and Jakowatz C V Jr 1994 Phase gradient autofocus—a robust tool for high resolution SAR phase correction *IEEE Trans. Aero. Electron. Syst.* **30** 827–35

[22]  Yazici B, Cheney M and Yarman C E 2006 Synthetic-aperture inversion in the presence of noise and clutter *Inverse Problems* **22** 1705–29

[23]  Ziomek L J 1985 *Underwater Acoustics: A Linear Systems Theory Approach* (Orlando, FL: Academic)